remote sensing

Article

Rooftop Photovoltaic Energy Production Estimations in India Using Remotely Sensed Data and Methods

Anil Kumar [1], Panagiotis Kosmopoulos [2,*], Yashwant Kashyap [1] and Rupam Gautam [3]

[1] Electrical and Electronics Engineering Department, National Institute of Technology Karnataka, Surathkal 575025, India; anilkumar.207ee002@nitk.edu.in (A.K.); yashwant.kashyap@nitk.edu.in (Y.K.)
[2] Institute of Environmental Research and Sustainable Development, National Observatory of Athens (IERSD/NOA), 15236 Athens, Greece
[3] CleanMax Solar Energy Solutions Ltd., Gurugram 122009, India; rupam.gautam@accenture.com
* Correspondence: pkosmo@noa.gr

Abstract: We investigate the possibility of estimating global horizontal irradiance (GHI) in parallel to photovoltaic (PV) power production in India using a radiative transfer model (RTM) called libRadtran fed with satellite information on the cloud and aerosol conditions. For the assessment of PV energy production, we exploited one year's (January–December 2018) ground-based real-time measurements of solar irradiation GHI via silicon irradiance sensors (Si sensor), along with cloud optical thickness (COT). The data used in this method was taken from two different sources, which are EUMETSAT's Meteosat Second Generation (MSG) and aerosol optical depth (AOD) from Copernicus Atmospheric Monitoring Services (CAMS). The COT and AOD are used as the main input parameters to the RTM along with other ones (such as solar zenith angle, Ångström exponent, single scattering albedo, etc.) in order to simulate the GHI under all sky, clear (no clouds), and clear-clean (no clouds and no aerosols) conditions. This enabled us to quantify the cloud modification factor (CMF) and aerosol modification factor (AMF), respectively. Subsequently, the whole simulation is compared with the actual recorded data at four solar power plants, i.e., Kazaria Thanagazi, Kazaria Ceramics, Chopanki, and Bhiwadi in the Alwar district of Rajasthan state, India. The maximum monthly average attenuation due to the clouds and aerosols are 24.4% and 11.3%, respectively. The energy and economic impact of clouds and aerosols are presented in terms of energy loss (EL) and financial loss (FL). We found that the maximum EL in the year 2018 due to clouds and aerosols were 458 kWh m^{-2} and 230 kWh m^{-2}, respectively, observed at Thanagazi location. The results of this study highlight the capabilities of Earth observations (EO), in terms not only of accuracy but also resolution, in precise quantification of atmospheric effect parameters. Simulations of PV energy production using EO data and techniques are therefore useful for real-time estimates of PV energy outputs and can improve energy management and production inspection. Success in such important venture, energy management, and production inspections will become much easier and more effective.

Keywords: global horizontal irradiance; cloud optical thickness; aerosol optical depth; radiative transfer model; cloud modification factor; aerosol modification factor

check for updates

Citation: Kumar, A.; Kosmopoulos, P.; Kashyap, Y.; Gautam, R. Rooftop Photovoltaic Energy Production Estimations in India Using Remotely Sensed Data and Methods. *Remote Sens.* **2023**, *15*, 3051. https://doi.org/10.3390/rs15123051

Academic Editor: Xuan Zhu

Received: 24 April 2023
Revised: 4 June 2023
Accepted: 8 June 2023
Published: 10 June 2023

1. Introduction

Due to the rapid population growth, vast development and growing energy demands are continuously putting pressure on the India's energy system. These growing needs of energy require a serious effort by the Government of India to augment its power supplies such as coal energy production. Renewable sources are much more viable than conventional methods as they are free from any greenhouse gas emissions [1–4]. Therefore, it is essential to develop cleaner and more reliable electricity [5–7]. Renewable energy sources contribute to securing the sustainable energy, which fosters economic growth [4,7–9]. Therefore, renewable energy has captured the interest of researchers and evolved enormously in last two decades [10,11].

In this context, a vision has been developed to promote renewable energy sources in order to decrease the dependency on non-renewable ones, along with carbon and greenhouse gas emissions [12]. Solar energy is one of the fast-growing industries across India. Based on International Renewable Energy Agency (IREA), India receives more than 5000 trillion kWh/year of solar radiation [13], which is a very large amount compared to the annual energy consumption. As per the latest energy statistics report of India, total energy consumption in India during the financial year 2021–2022 is 33,508 PJ [14]. Therefore, this stock can be used for concentrated solar power plants (CSP) and PV energy production. Jawaharlal Nehru National Solar Mission (JNNSM) or National Solar Mission (NSM) is one of the initiatives from the government of India (https://www.iea.org/policies/4916-jawaharlal-nehru-national-solar-mission-phase-i-ii-and-iii; assessed on 14 January 2022) focused towards installations of 5 GW grid connected solar power project under phase II of the JNNSM. The JNNSM has been revised and targeted to the deployment of 100 GW of grid-connected solar PV power, which includes 40 GW of grid-connected rooftop solar installations by 2022 [15]. A detailed overview of the solar energy developments over the Indian subcontinent is presented in several earlier papers [3,7,15–17].

The rooftops photovoltaics studied are directly related to urban planning in order to promote the PV penetration at an urban environment and scale for energy transition policies and decision making. As time progresses, urbanization and economic developments in India are resulting in a substantial rise in energy demand. However, this escalating demand is significantly contributing to the emissions of greenhouse gases. The increasing energy demands pose a considerable challenge for local governments to meet the demand due to electricity shortages in most of the cities. The "Solar Cities" program is launched with the objective to support the local urban bodies to guide their cities towards a transition to renewable energy sources. The government of India has introduced several initiatives targeting the urban sector to promote the development of rooftop systems; widespread adoption of solar water heating systems, "Akshaya Urja Shops", is a notable initiative that promoted the urban industrial waste and biomass to energy projects [18]. In 2015, the government of India launched the "Smart Cities Mission" with the objective of transforming urban areas to be energy efficient so that the energy burden on existing resources can be reduced. Under this mission, the target was to make 80% of smart city buildings energy efficient, with 10% of the energy being met through solar energy resources [19]. Prior to achieving such goals, study of atmospheric parameters (i.e., aerosols, clouds) is crucial for estimating the solar radiation levels in a given place.

This decrease in the amount of solar radiation reaching the Earth's surface (SSR) has significant impact on our electrical budget, alongside the hydrological cycle [20–23]. The reduction of SSR due to the attenuation of global horizontal irradiance (GHI) and beam horizontal irradiance (BHI) leads to reduction in the efficiency in solar power plants and PV energy production. Atmospheric aerosols and clouds are the most important factors in solar irradiation extinction. The impact of aerosols and clouds on solar energy production is presented in [17,24] but none of these parameters are accurately measured with ground based measurements. Instead, Earth Observation data sources were used for continuous monitoring, modelling, and forecasting of these parameters. So, a big effort has been performed worldwide over the last years in order to make such observations as reliable as possible. With this background information, the current work investigates the possibility of estimating the GHI and PV power production in India using a radiative transfer model (RTM) fed with Earth observation (EO) information on clouds and aerosols' conditions and validated using real-time ground-measured GHI measurements. The novel features of our proposed study are summarized as follows.

The study of urban planning and the possibilities for placing PVs on the roofs of the buildings, in combination with the control and management of the supply and demand of energy, are a concern for the transformation of cities into smart cities. As a result, cities and urban areas are key players in climate change, since they consume more than two-thirds of the world's total energy need and are responsible for all global greenhouse gases emissions and such, must be included to cities energy planning. The quantification of the atmospheric parameters effect on solar energy production, as well as the urban environment effects, is a key to this direction, while the ultimate goal is to support and contribute to the worldwide effort of developing real-time decision-making instruments by exploiting all the modern available methods, Earth Observation data sources, and technologies.

The remaining part of this study is structured as follows: the study sites, rooftop PV system, solar sensor data, COT, and AOD data used in this study are presented in Section 2.1, followed by the methodology in Section 2.2, which includes radiative transfer model simulation, solar energy simulation, and financial aspects. The results are presented in Section 3 which includes the impact of clouds and aerosols on all sky GHI, the comparison of AMF and CMF, real time and simulated PV comparisons, and economic impact due to aerosols and clouds, followed by the capabilities and limitations of EO. Finally, the conclusions are presented in Section 4.

2. Materials and Methods

2.1. Materials

2.1.1. Study Site

The study locations are in Rajasthan's Alwar district, which receives huge quantities of solar radiation. Alwar is oriented in the North-East of Rajasthan between 27.34° and 28.4°N latitude and 76.7° and 77.13°E longitude. The district is located between the Yamuna-Satluj divide and the central part of the district is covered by the Aravalli hills, which run north-south ranging in height from 456 m to 700 m. In a year, Rajasthan has approximately 300–330 days of clear sunshine. The clear sunshine days are an important indicator of the amount of sunlight that reaches the Earth's surface, but they do not provide a complete picture of air quality. Air pollution can have a number of sources, including emissions from transportation, industry, and biomass burning, etc. The state has installed 7738 MW solar power capacity from ground mounted and 545 MW solar power capacity from rooftop under the net metering scheme, as per the record of Rajasthan Renewable Energy Corporation Limited (RRECL) till September 2021 (last accessed on 14 July 2022: https://energy.rajasthan.gov.in/content/raj/energy-department/rrecl/en/home.html).

Solar energy received in India depends on geographical conditions, however, Rajasthan and Northern Gujarat are the states that receive the highest global radiation, which is more than 2400 kWh m^{-2} [10] annually. Figure 1 shows the sites under investigation, i.e., Thanagazi (27.4°N, 76.313°E), Ceramics (28.05°N 76.83°E), Chopanki (28.195°N 76.864°E), and Bhiwadi (28.195°N 76.864°E) in Alwar, the other parameters details for these study sites are listed in Table 1. Figure 1 enables readers to see more details about the region, to understand the morphology and the reasons for the use of EO-based solar energy planning tools and methods.

Figure 2 shows the roof-top image of all four stations, which is Trina's designed solar modules. At the Thanagazi plant the solar modules are spread over 8237 m^2 and installed at a tilt of 7°. The DC nominal power rating for this station is 1504 kWp and AC nominal power rating is 1175 kW. All such parameters for other stations are available in Table 1.

2.1.2. Silicon Sensor for Ground-Based Data Measurement

A year-long real-time measurement of ground-based solar radiation GHI data from four stations (Table 1) has been used to study photovoltaic energy production comparison. The silicon (Si) sensor of type Si-V-10TC-T is used for ground-based GHI measurements. The Si-V-10TC-T Si sensor is used as an irradiance sensor because the short-circuit current is proportional to irradiance. The elements of the sensor are designed in a certain way, ideal for monitoring the PV system (https://www.imt-solar.com/solar-irradiance-sensors/: last accessed on 17 February 2022). A Si sensor is made up of mono-crystalline Si solar cells which are reliable, robust, and economical elements. The acronym "TC "in the Si solar sensor signifies the active temperature compensation measured by an equivalent sensor laminated to the back section of the solar cell for minimizing the effect of temperature on the measuring signal. All sensors are calibrated in artificial sunlight against a reference cell calibrated at the Physikalisch-Technische Bundesanstalt (PTB, 147 National Metrology Institute of Germany) (https://www.ptb.de/cms/en.html, accessed on 9 June 2023).

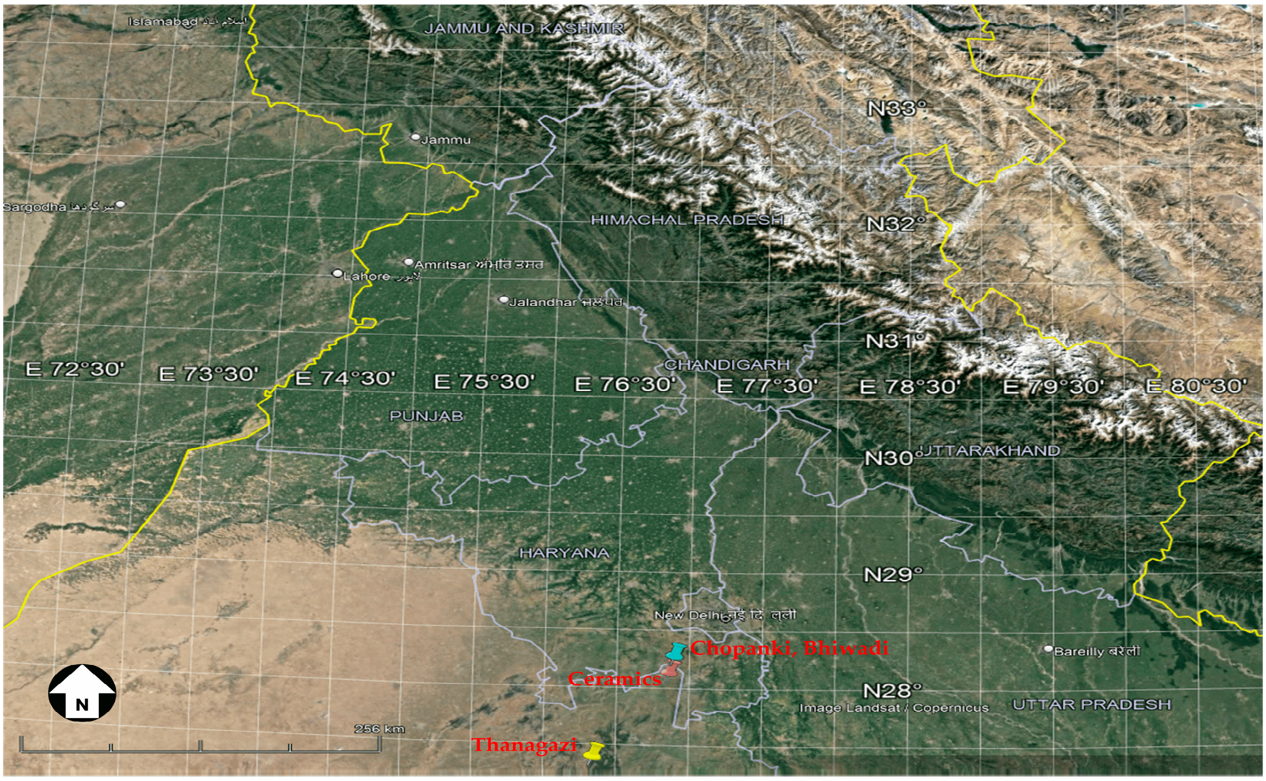

Figure 1. Location map of experimental site in Alwar (taken from Google Earth).

Table 1. Indian solar farm stations used in the study.

Station	Lat (°N)	Long (°E)	DC Nominal Power (kWp)	AC Nominal Power (kW)	Module Area (m^2)	Altitude (m.a.s.l)	Tilt (°)
Thanagazi	27.313	76.313	1504	1175	8237	447	7
Ceramics	28.05	76.83	1354	1080	7496	280	6
Chopanki	28.195	76.864	1008	775	5467	290	10
Bhiwadi	28.195	76.864	1004	800	5608	260	6

2.1.3. Cloud Data

Satellite cloud data product is one of the important inputs for our model simulation, these were obtained from the Spinning Enhanced Visible and Infrared Imager (SEVERI) on board the MSG. To accurately measure the impact of clouds on solar irradiation, we collected data on cloud type (CT), cloud phase (CP), and cloud optical thickness (COT). The CP helps to identify whether or not a simulated cloud pixel has an ice or water radiative transfer characteristic, CT makes it possible to determine their height and effective radius, whereas COT enables for the measurement of incoming solar radiation attenuation. COT is influenced by cloud vertical thickness as well as moisture density. The reflectance feature of cloud at channel at 0.6 μm in visible region of the electromagnetic spectrum closely associated with COT [25]. The EUMETSAT's MSG is a geostationary meteorological satellite that is present at 36,000 km above the equator allows for continuous monitoring of Europe, Africa, and the Indian Ocean (45°E) at the high spatial and temporal resolution of 0.05° and 15 min respectively. The real time cloud properties were extracted using Satellite Application Facility for Nowcasting Weather Conditions software (SAFNWC) installed in-house. CT and CP are conventional outcomes of the SAFNWC computational technique, whereas COT is a customized product and so its extraction needs additional steps in the process chain. The MSG product identification is described in [26] technical report.

Figure 2. Rooftop image of solar farms in Alwar district of Rajasthan state.

2.1.4. Aerosol Data

AOD is a dimensionless indicator of the direct solar irradiation attenuation at ground level due to particulate matter. The AOD_{550} data was obtained from CAMS which provides AOD forecasting information for the next day in spatial and temporal resolutions of 0.4° and 1 h, respectively. The CAMS is a service run by the European Centre for Medium-Range Weather Forecasts (ECMWF) on behalf of the European commission under Copernicus program [27]. The CAMS dataset contains aerosol modeling and satellite data assimilation with the modeling part based on ECMWF physical parameterizations of aerosol processes. They give operationally correct aerosol optical depth (AOD) data at 550 nm, 1 h time steps, and 0.4° spatial resolution. For our model simulation to estimate GHI together with PV production, AOD and COT are the two main input parameters for RTM simulation. All four plant regions were found to have AOD values that ranged from 0.1384 to 3.5522 over the course of a year.

2.2. Methodology

2.2.1. Radiative Transfer Model Simulation

The real time assessment of GHI and PV production is based on Look-up tables (LUTs), calculated using RTM (libRadtran) [28–30]. The LUTs consist of more than 2.5 million RTM simulations with atmospheric inputs and 1 nm spectral GHI outputs. A study was conducted to investigate the interoperable exchange of the same kind of GHI databases [31], emphasizing the importance of LUTs methods [32]. As presented in [33], the size of LUTs is large but still it provides estimated values for discrete points, so for real world application this needs to generate an interpolating function to be applied for nearest/adjacent LUTs values to correct the input output parameters. However, it is found that the interpolation calculation process is computationally expensive and approximately requires a total time of 21 h. Each interpolation calculation took more time than a single run of libRadtran, which was initially used to generate the LUTs in the first place, which was approximately 12 h for 1000 RTM simulations. In this direction, 2.5 million records of LUTs [34] were used for fast retrieval of solar radiation levels. The outputs are high-resolution spectral irradiances (1 nm) covering the wavelength range of 285 to 2700 nm. The parameters and their value range that are allowed to vary in 2.5 million simulations for the purposes of this study are cloud optical thickness (0:0.1:5 and 5:1:20), aerosol optical depth (0:0.1:2.5), Ångström exponent (0.2:0.6:2), single scattering albedo (0.6:0.2:1), water vapor (0.5:1:3.5) (measured in cm) and solar zenith angle (1:3:88). In more detail, we used the RTM called SDISORT which is a pseudospherical analog of the DISORT solver described in [35] and it ensures that the outputs in terms of spectral GHI are valid from 0 to 90° solar zenith angle (SZA). More clearly, we can say the model used is the SDISORT which can be found in the libRadtran which acts as a library of RTM and methods. Concerning the way of RTM simulations, we selected the band parameterization based on the correlated-k approximation [36,37], whereas the aerosol and cloud determination was conducted based on the predefined aerosol framework explained in [38]. All the scientific and structural details about the RTM simulations, the input datasets and the LUTs construction are described in [33].

The outcomes of the above RTM procedure are estimated GHI obtained by using AOD and COT as the main input parameter to RTM (libRadtran) at 550 nm wavelength and this was extrapolated to the whole solar spectrum used in this study. In detail, AOD, SZA, Ångström exponent (AE), single scattering albedo (SSA), total ozone column (TOC), and columnar water vapor (CWV) were used as input parameters in libRadtran under clear sky, whereas SZA, TOC, and COT are used under cloudy sky condition for GHI estimation. AOD is not used as input in libRadtran under the cloudy condition when COT is greater than unity because the effect of aerosol is much weaker in comparison to thick clouds (i.e., COT > 1). The additional parameters consist of the SZA which was collected from an in-house astronomical model and software (NOA), AE, SSA from the Aerosol Comparisons between Observations and Models (Aerocom) [39] on a monthly average basis, the TOC from Tropospheric Emission Monitoring Internet Service (TEMIS) [40] once per day, and the CWV from CAMS respectively. The standards atmosphere effect to solar radiation as compared to other atmospheres motives is directly related to the attenuation due to atmospheric gases, while for the standard aerosol selection the influence is related to the handling of the optical properties in terms of optical depth, Angstrom, single scattering albedo etc. For the RTM simulations, the standard atmosphere [41] and the default aerosol model [38] were used, while the uncertainty effect on solar irradiation under various molecular bands parameterization and aerosol typing is able to reach up to 60% under extreme atmospheric conditions and aerosol vertical distribution [42,43]. Using the aforementioned RTM process, we simulated GHI under three different conditions: clean and clear (no aerosols and no clouds; $GHI_{clean\ \&\ clear\ sky}$), clear (no clouds; $GHI_{clear\ sky}$) and all sky (real condition; $GHI_{all\ sky}$). Where clear sky means that it is cloudless, while a clean and clear sky means it is free from aerosols and clouds.

2.2.2. Solar Energy Simulation and Financial Aspects

The solar irradiance that reaches on the PV panels must be known to estimate the power output from solar farm systems. To obtain solar radiation data, PV energy production and to determine necessary numerical calculation, we utilized the Photovoltaic Geographic Information System (PVGIS) [44]. It is very crucial to understand the entire system losses based on actual solar application scenarios. Aerosols and clouds are key players that contribute significantly to loss of solar energy. An environment with an AOD value of 0.01 would be highly clean, whereas one with a value of 0.4 would be very hazy condition [45,46]. Clouds do not absorb visible light wavelengths but rather scatter and reflect the majority of visible light. The aerosol and cloud influence on solar energy can be expressed by the

AMF and CMF, which is computed by the formula expressed in Equations (1) and (2) and explained in reference [17]:

$$\mathrm{AMF} = \mathrm{GHI}_{\text{clear sky}} / \mathrm{GHI}_{\text{clean \& clear sky}} \quad (1)$$

$$\mathrm{CMF} = \mathrm{GHI}_{\text{all sky}} / \mathrm{GHI}_{\text{clear sky}} \quad (2)$$

where $\mathrm{GHI}_{\text{clear sky}}$ is the radiation under clear sky conditions, $\mathrm{GHI}_{\text{clean \& clear sky}}$ is radiation under clean (from aerosols) and clear (from clouds) sky conditions and $\mathrm{GHI}_{\text{all sky}}$ is radiation under all sky conditions. The abovementioned AMF and CMF variables have values ranging from 0 to 1, with 1 representing clear sky $\mathrm{GHI}_{\text{clear sky}}$ (i.e., no cloud effect) and all lower values showing $\mathrm{GHI}_{\text{all sky}}$ with cloud effect. Similarly, the $\mathrm{GHI}_{\text{clean \& clear sky}}$ with 1 value shows clean and clear sky irradiation. This approach allows for the evaluation of the independent effects of aerosols and clouds on solar energy. So, we can calculate the attenuation in GHI due to aerosols and clouds using AMF and CMF expressions. The percentage attenuation in GHI due to clouds is $((\mathrm{GHI}_{\text{all sky}} - \mathrm{GHI}_{\text{clear sky}})/\mathrm{GHI}_{\text{clear sky}}) \times 100$ while the corresponding attenuation due to aerosols is $((\mathrm{GHI}_{\text{clear}} - \mathrm{GHI}_{\text{clean \& clear}})/\mathrm{GHI}_{\text{clean \& clear}}) \times 100$. The aforementioned equation by replacing with CMF and AMF definitions are: (CMF-1) $\times$ 100 and (AMF-1) $\times$ 100. We have shown the annual variation (January–December 2018) of CMF (Figure 3) and AMF (Figure 4) as it includes cloud optical thickness and aerosol optical depth, and all the other parameters are included by default into the above quantities since for example the ice clouds have a larger impact on solar radiation than water clouds. At the same time the cloud optical thickness due to ice crystals is lower than due to water droplets and is related to the monsoon characteristics and microphysics. To this direction the parameters that make sense to see the annual cycle are the CMF and AMF as shown in Figures 3 and 4 respectively.

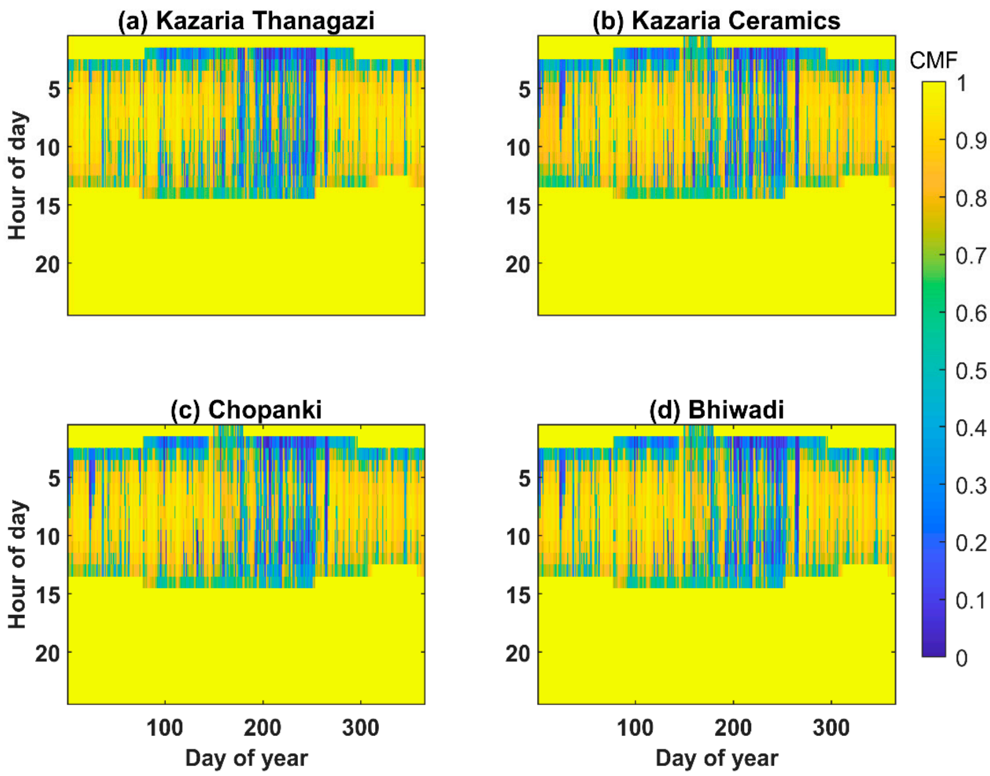

Figure 3. Annual variation in CMF for all four stations in Alwar.

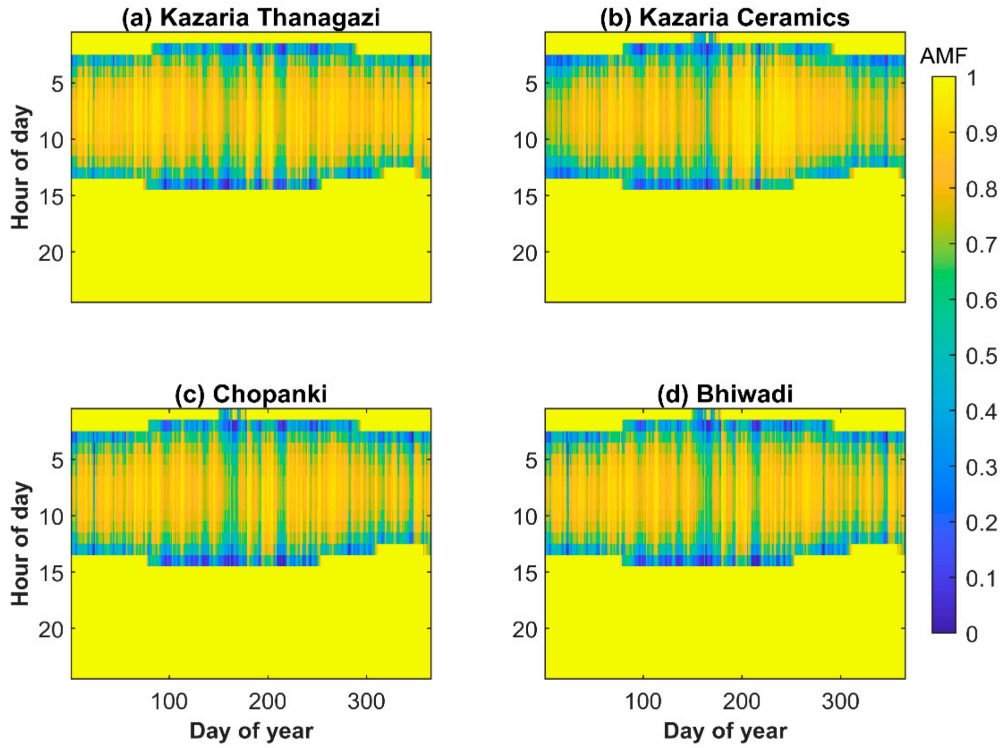

Figure 4. Annual variation in AMF for all four stations in Alwar.

Financial analysis shows the limitations of EO data and simulation to represent the reality of PV production and its losses due to atmospheric aerosols and clouds. To this direction, the financial analysis is able to represent the magnitude of the simulations ability to be efficiently translated into realistic solar energy estimations. The financial analysis was carried out by simulating a hypothetical scenario of a PV system with nominal power of 1 MW assumed to be installed in Alwar using the methodology stated in [17]. For the estimations of solar PV energy production, the most prevalent PV materials were simulated with an average efficiency of 16% and at the same time the shadowing impact from the surroundings was set to 4% as a representative value unimpeded from the visual horizon solar plant installations. As a result, the remaining 80% efficiency has been transformed to PV output energy using nominal power and electricity converter technology, as well as AC/DC efficiency. The financial analysis of PV energy production requires the electricity generation price INR per kWh (1 INR ≈ 0.013 USD); then the PV output energy is converted into the price of electricity as follows the earlier energy by [17]. Financial analysis was formulated in terms of energy production (Ep), revenue generated (RG), and financial losses (FL). Ep was obtained as the sum of generated energy in kWh/m^2. RG is obtained by feed-in tariff price multiplied by Ep as shown in Equation (3).

$$\text{RG} = \text{Ep (kWh)} \times \text{price of electricity} \left(\frac{INR}{\text{kWh}}\right) \tag{3}$$

The price of electricity in the present work was taken as 3.14 INR/kWh for India [47] up to the capacity of 725 MW and hence the financial loss is calculated using Equation (4)

$$FL\ (INR) = (\text{Ep}_{max} - \text{Ep}_{actual}) \times \text{price of electricity} \tag{4}$$

where, Ep_{max} is the maximum energy produced under clear sky conditions i.e., AOD and COT value is zero and Ep_{actual} is the actual value of energy produced in kWh in which the AOD value was taken into consideration under clear sky conditions, and COT value under cloudy sky conditions.

3. Results

3.1. Impact of Clouds and Aerosols on All Sky GHI

Figure 5 shows the diurnal variation in GHI observed at all four stations located in Alwar, throughout the day from January to December 2018 under all sky conditions. All sky GHI variation in Figure 5 over different seasons is justified as per study conducted for central Himalaya region of India [17]. It is worth noting that the presented GHI data in Figure 5 only covers the time period from 0 to 14 h of the day, as the GHI values during the remaining hours of the day (15–24) under all-sky conditions were registered as zero in the RTM outputs. The time standard used for this study is Coordinated Universal Time (UTC). The diurnal GHI variation at all four stations exhibits a peak of 1000 W m^{-2} to 1200 W m^{-2} occurring between 6 to 10 h of the day during the month of April (i.e., 91–120 day of year), May (i.e., 121–151 day of year) and June (i.e., 152–181 day of year). However, during the Indian summer monsoon which spans from July (i.e., 182–212 day of year) to August (i.e., 213–243 day of year) the GHI values demonstrate a discernible decline due to increased cloud cover and hence lower GHI values is observed as presented in [15]. Meanwhile, autumn and winter months show lower values of GHI, as expected. The insight provided above offers a comprehensive understanding of temporal variability of GHI at different locations in Alwar, across different seasons of a year.

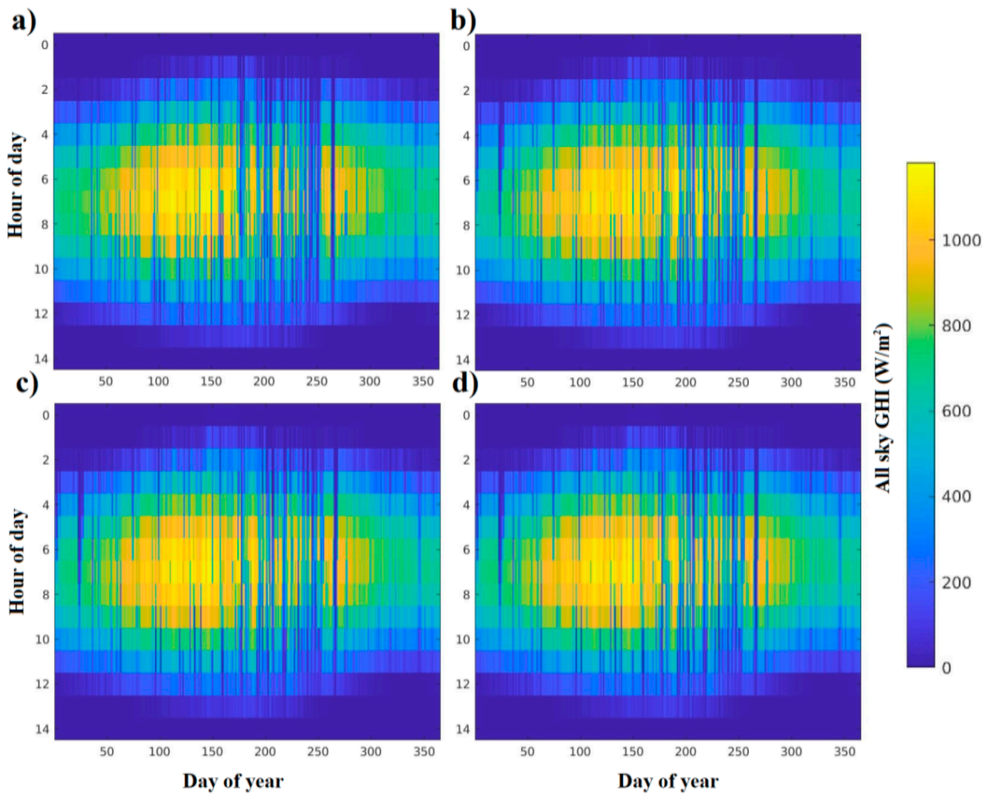

Figure 5. Contour plot of GHI under all sky condition simulated using RTM for all four stations. (**a**) Thanagazi (**b**) Ceramics (**c**) Chopanki (**d**) Bhiwadi.

3.2. Comparison of AMF and CMF

The impact of aerosols and clouds on solar energy can be quantified using the parameter AMF and CMF respectively and it is recently studied for the Himalayas region in India [17]. Figure 6 shows the monthly variation in AMF and CMF for the four sites we examined in Alwar. The monthly variability of CMF is obtained by utilizing 15-min samples of COT, following the same frequency as that of AOD time series data, which is measured at an interval of 1 h. Simultaneously, AMF curves were computed based on hourly measurements of the AOD data. CMF shows a gradual increment before and after the monsoon (July, August, September) signifies that the effects of clouds are minor, whereas, during the monsoon, the lowest values of CMF are observed attributes for huge cloud coverage. The monthly variation in CMF values ranges from 0.50 to 0.95. However, the AMF exhibits unpredictable changes over the course of a year, characterized by sharp fluctuations. The attainment of the highest AMF climatological values during the winter and spring consequently signifies minor aerosols effect whereas the lowest AMF climatological values are observed in months of July signify for higher aerosols effect. These values could be attributed due to the displacement of dust aerosols from the West Asian region [16,17,48]. After the necessary calculations, it is proven that the AMF and CMF at all these four stations are comparable which is an important finding for India because accurate measurement of both these quantities is crucial when calculating the solar radiation losses, as well as determining the total energy output of a PV system.

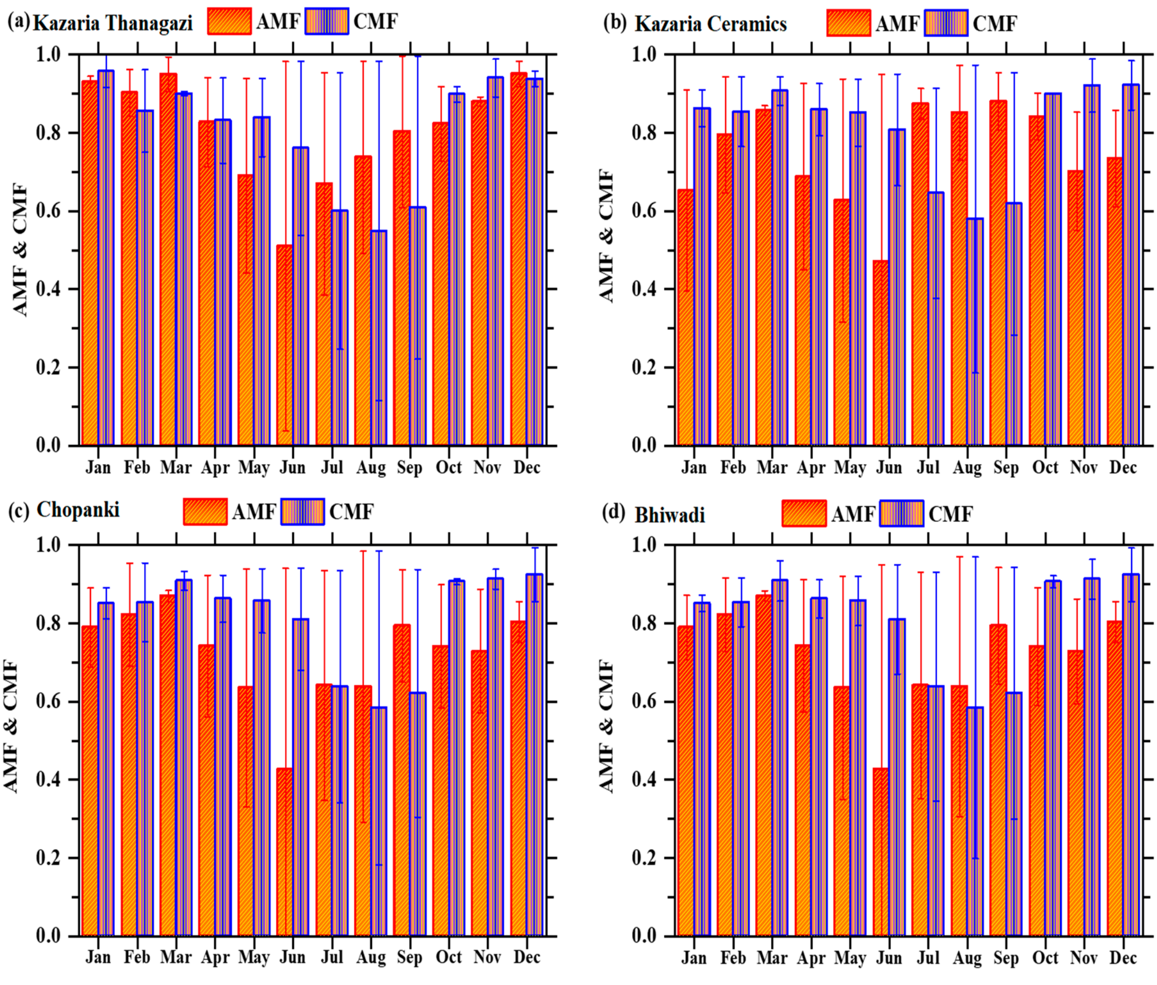

Figure 6. Comparison of AMF and CMF at four locations (**a**) Kazaria Thanagazi (**b**) Kazaria Ceramics (**c**) Chopanki (**d**) Bhiwadi.

Figure 7 emphasizes the absolute value of the percentage attenuation in GHI resulting from AMF and CMF. RTM simulations yielded these results. The losses due to AMF include the aerosol effect, whereas the losses due to CMF only include the cloud effects. Studies conducted in other regions [15] suggest that generally the impact of aerosol is more stable than that of clouds over the course of a year. Therefore, the losses resulting from AOD do not have significant changes when compared to losses caused by clouds, which display substantial fluctuations, as shown in Figure 7. In Figure 7 the interquartile range within the box is between 25th and 75th percentile to show the median whereas the vertical solid lines show the upper whiskers which represents the maximum attenuation in GHI due to aerosols and clouds. Attenuation due to clouds is observed during summer and early winter due to monsoon activity whereas attenuation due to aerosols is common during all seasons as aerosol behavior is related to human activities or dust as well. A major attenuation in GHI radiation due to clouds is seen during the month of July, August, and September because of dense cloud cover due to monsoon activities in Alwar. Since the cloud cover is not very dense in other seasons no attenuation in GHI radiation is observed. In the case of reduction due clouds, the largest interquartile difference is observed for Thanagazi whereas in case of lessening in GHI due to aerosols the maximum interquartile separation is observed for Chopanki and Bhiwadi location. In literature [49], Iqbal method [50] was employed to estimate solar irradiance, taking into consideration the impact of total optical thickness determined by AERONET. The author demonstrated that in a cloudless atmosphere, the incident solar irradiance is attenuated by 23.5%, with aerosols accounting for an average contribution of 13.5%. In literature [51], the Iqbal model C has been utilized for GHI estimation and analysis conducted over several years showed that annual average deviation ranged from 8.7% to 19.2%. Our proposed RTM method fed with EO data got average annual percentage attenuation in GHI ranges from 9% to 10% attributable due to cloud variations across the four different locations in Alwar. Additionally, the annual average attenuation in GHI resulting from aerosols is observed between 5% to 7%. So, our finding is justified as per the previous literature. The maximum monthly average attenuation in GHI due to aerosols for Thanagazi, Ceramics, Chopanki, and Bhiwadi locations are 9.4%, 10.5%, 11.3%, and 11.3% respectively noticed during June whereas the maximum monthly average attenuation in GHI due to cloud is 24.4%, 22.8%, 22.5%, and 22.5% respectively noticed during August.

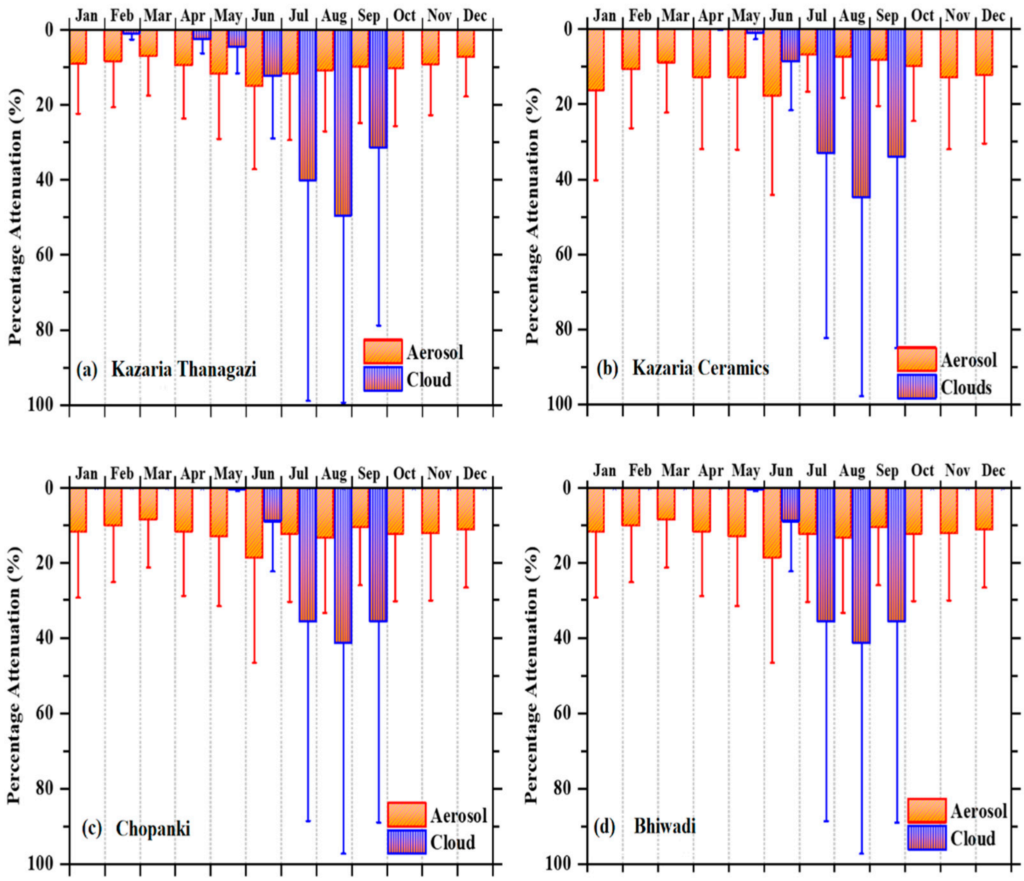

Figure 7. Box plot for the percentage attenuation in GHI due to aerosols and clouds for (**a**) Kazaria Thanagazi (**b**) Kazaria Ceramics (**c**) Chopanki (**d**) Bhiwadi.

3.3. Real Time and Simulated PV Comparisons

We made the comparison between the GHI under three different conditions i.e., $GHI_{clean\ \&\ clear\ sky}$, $GHI_{clear\ sky}$, $GHI_{all\ sky}$ along-with the simulated PV and the real-time ground-truth measured GHI radiation for all the four stations in Alwar as shown in Figure 8. Real PV in Figure 8 is measured GHI, which was used in order to quantify the reliability of the simulations performed. The accuracy of the estimated GHI has been tested and validated against real time ground measured GHI measurements [52]. These measurements are represented in Figure 8 as black line plot, labeled as "Real PV". The simulations were compared with the real PV measurements, and the accuracy of the estimated GHI was evaluated based on how closely it matched with real PV data. The $GHI_{clean\ \&\ clear\ sky}$ (i.e., GHI_0; red color) shows the highest values during the summer months. Among all the four farms, the maximum value (311 kWh m^{-2}) of GHI_0 is obtained during July whereas the minimum values (150 kWh m^{-2}, 147 kWh m^{-2}, 146 kWh m^{-2}, and 146 kWh m^{-2}, respectively for Thanagazi, Ceramics, Chopanki, and Bhiwadi) during the month of December as depicted in Figure 8. The simulated GHI under cloud free sky conditions (GHI_{AMF}; green color) shows quite similar variations with slightly lower values (Figure 8), which clearly indicates that the effects of aerosols do not dominate in these locations of Alwar. In a parallel manner, the simulated GHI under all sky conditions (GHI_{CMF}; represented by blue color) shows similar monthly variation with the simulated PV for all four solar power plants, which suggests that clouds play a bigger role than aerosols (Figure 8). During monsoon months, the GHI_{CMF}, simulated PV as well as real-time GHI (Real PV) measurements show a drop due to the significant cloud coverage over all four solar farm locations. The comparison between the GHI under different conditions clearly shows the accuracy of the model simulations which are quite suitable for real-time PV investigations. In addition, in Figure 8 the simulated PV (shown by cyan color) with the tilt angle of the PV panel is found to match very well with the real-time PV (measured GHI) measurements. However, the simulated PV data overestimate real-time PV due to some technical issues such as panels soiling, maintenance, inverter, ac-dc conversion efficiency, remote sensing data information resolution and subsequent uncertainties, panel efficiency, possible failures following with temperature and shadow effect.

The tilt angle is one of the most important parameters for the calculation of solar PV power. To optimize the annual production of solar energy for fixed non tracking solar PV panels, the tilt angle is a few degrees below the latitude of the site. Therefore, in the present work, we selected the tilt angle for Thanagazi, Ceramics, Chopanki, and Bhiwadi at 7°, 6°, 10° and 6° respectively. Figure 9 illustrates the monthly mean variation in percentage increase in PV production resulting from different tilt angles. Figure 9 depicts that for Thanagazi, the tilt angle of 10° results in maximum PV production increase, reaching as high as 20% during the month of December. On the other hand, the lower tilt angles of (6–7°) for Ceramics, Chopanki and Bhiwadi results in 10% to 14% maximum PV production increase which is observed in months of December. Figure 9 clearly indicates that the percentage PV power production increase is very sensitive to the small changes in the tilt angle observed over a course of year. Figure 9 also clearly reveals that the tilted PV panels produce more energy but not during all the months. During April, May, June, and July, PV energy production remains the same for every tilted angle. This could be an attribute of the significant dominance of cloud coverage and hence the presence of maximum diffuse radiation.

3.4. Economic Impact Due to Aerosols and Clouds

Figure 10, shows the economic analysis of the impact from aerosols and clouds on solar energy production, quantified in terms of monthly mean along with total energy and financial losses. The associated methodology is described in Section 2.2.2 and also available in [53]. The monthly PV production and revenue for four locations are shown in Figure 10. For Thanagazi solar plant, the monthly mean PV energy varies from 107 kWh m^{-2} to 198 kWh m^{-2} from January to May in the year 2018 and followed by a decrease from

187 kWh m^{-2} to 97 kWh m^{-2} from June to December (Figure 10a). A similar variation in PV energy production is clearly visible for all four solar power plants which are shown in Figure 10. The total annual PV energy production (Ep), corresponding annual revenue, energy loss due to aerosols ($EL_{aerosol}$), energy loss due to clouds (EL_{cloud}), financial loss due to aerosols ($FL_{aerosol}$) and financial loss due to clouds (FL_{clouds}) for all four stations are summarized in Table 2. These costs also include the general inspections, system cleaning, mechanical maintenance, mounting, local taxes, site security and administration costs [54].

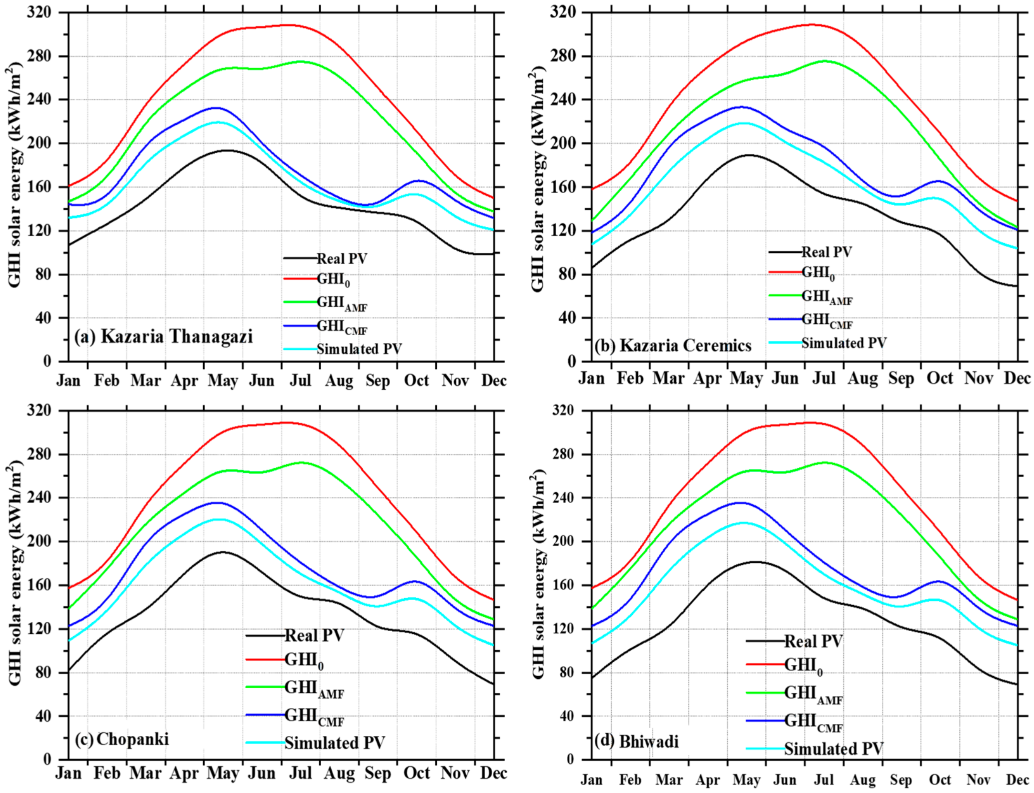

Figure 8. Comparison plot of real PV (black color) with simulated GHI under clean and clear sky (GHI_0; red color), GHI under clear sky (GHI AMF; green color), GHI under all sky (GHI CMF; blue color) and simulated PV (cyan color) for four locations in Alwar (**a**) Kazaria Thanagazi (**b**) Kazaria Ceramics (**c**) Chopanki (**d**) Bhiwadi.

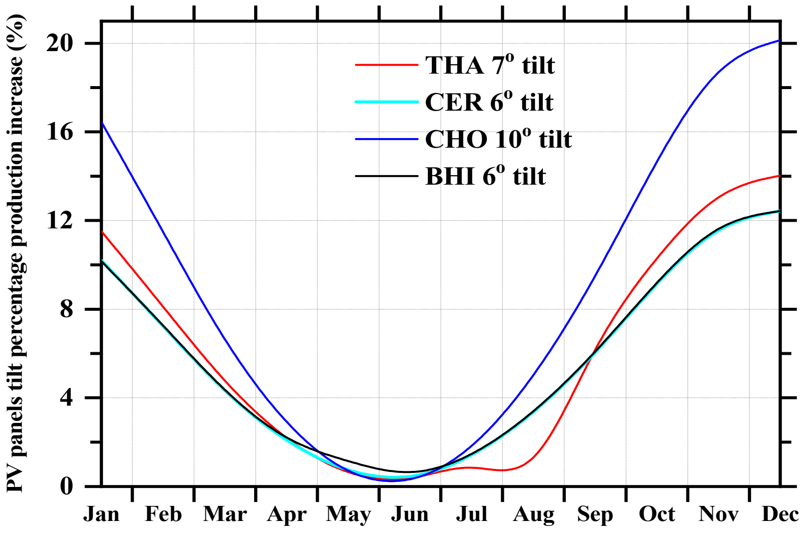

Figure 9. Percentage of PV production increase over a year for different tilt angles.

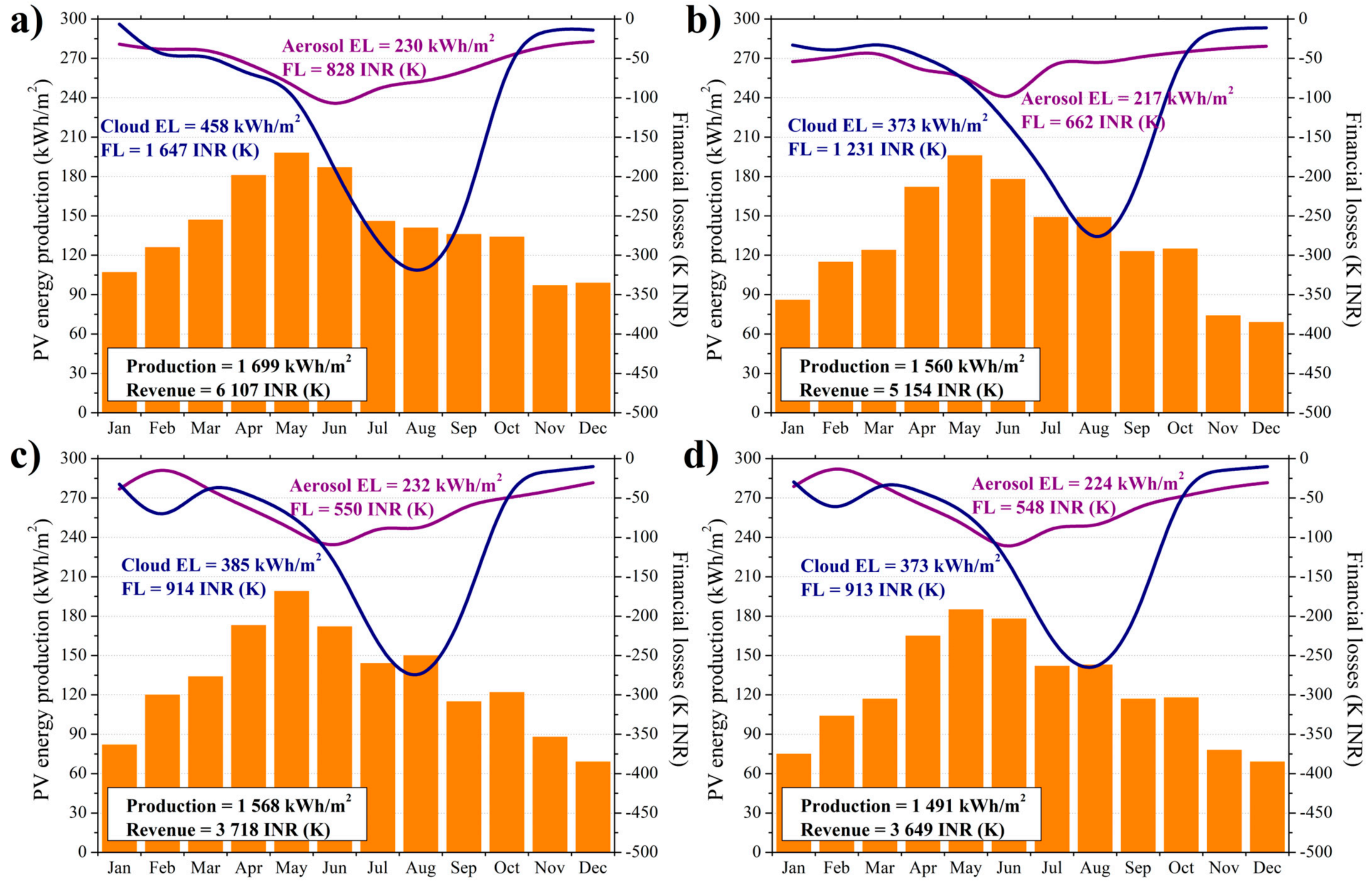

Figure 10. Economic analysis and revenue at four stations (**a**) Thanagazi (**b**) Ceramics (**c**) Chopanki (**d**) Bhiwadi.

Table 2. Annual energy production, revenue, EL and FL results for all four stations.

Stations	Ep (kWh m^{-2})	Revenue (K INR)	EL$_{aerosol}$ (kWh m^{-2})	EL$_{cloud}$ (kWh m^{-2})	FL$_{aerosol}$ (K INR)	FL$_{cloud}$ (K INR)
Thanagazi	1699	6107	230	458	828	1647
Ceramics	1560	5154	217	373	662	1231
Chopanki	1568	3178	232	358	550	914
Bhiwadi	1491	3649	224	373	548	913

Moreover, we have estimated the energy production loss error and financial loss error due to clouds and aerosols for all four solar plants (Figure 11). Figure 11 shows the limitations of EO data and simulation to represent the reality into PV production and its losses due to atmospheric aerosols and clouds. In [55] the author has proved that the uncertainties in the indirect effect of aerosol can be minimized with detailed measurements of atmospheric aerosols and cloud properties. For this we need to establish several observations all over India with the purpose to carry out in-situ measurement of cloud parameters as well as chemical compositions, mixing state alongside with size and shape of aerosol particles. In [56] author has shown the comparison between AOD obtained from MODIS with the AERONET. As it is obvious, there is a large uncertainty between the two data sources. This demands an AOD retrieval system with better spatial resolution and more accuracy with complex climatology. This will greatly improve our satellite-based estimations.

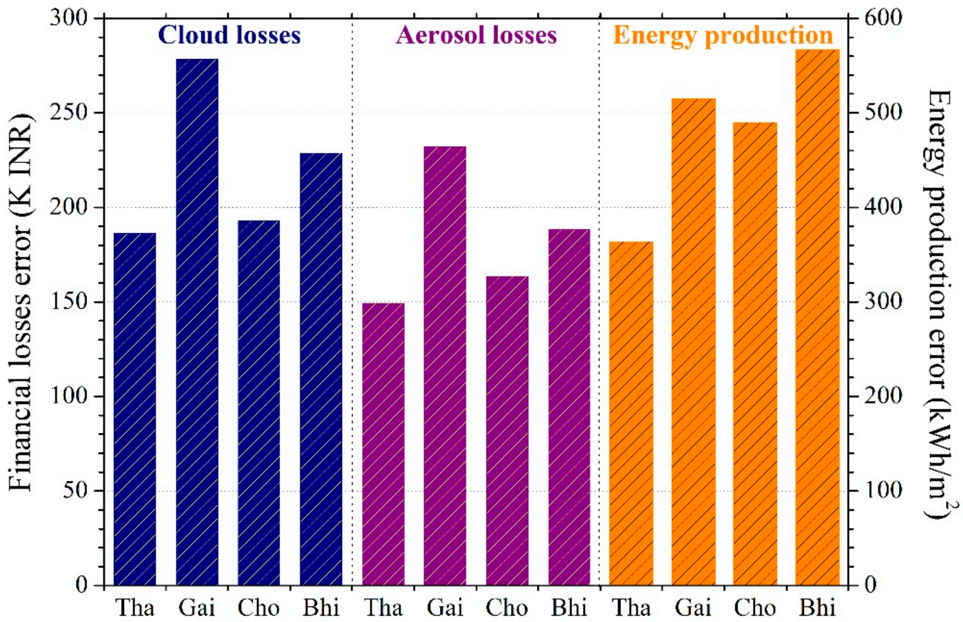

Figure 11. Energy production error (kWh/m^2) and financial loss error (K INR) for Thanagazi, Ceramics, Chopanki, Bhiwadi.

The capabilities as well as the limitations of modern EO to simulate the PV energy production over India in addition to the impact of atmospheric aerosols and clouds on GHI make us retrieve the COT from MSG and AOD from CAMS. The COT and AOD are used as two main input parameters for RTM simulation to find the GHI under all sky and clear sky conditions and also to quantify the CMF for all four locations. We have also investigated that the contribution of the Thanagazi plant is close to 70% of total consumption. This study tries to harmonize the ground-truth solar irradiation and production data with the modelled ones by exploiting exclusively Earth-Observation data and methods. The region of southern Asia is not sufficiently covered in terms of solar irradiation monitoring and forecasting management, while at the same time India presents one of the highest solar energy production levels from big solar farms to small and medium rooftop photovoltaic installations at urban scale and environment. To this direction, the study of the atmospheric parameters effect on the energy captured by the photovoltaics is crucial for efficient energy planning and decision making. However, in order to simulate real-time PV energy production, we have certain capabilities and limitations in our approach. The capabilities are continuous monitoring since the MSG is a geostationary satellite. CAMS provides modeled aerosol information continuously from satellites. Furthermore, the RTM converts the atmospheric inputs into solar radiation and so we can estimate the PV energy production. Capabilities have to do with a realistic estimation of the PV energy production by using exclusively EO data and techniques. This capability enables the harmonization of real-time PV energy outputs with the simulations and once succeeded, it performs energy management and production inspection (e.g., organizing the panels, cleaning and limit electricity outages due to previous knowledge of the clouds and aerosols effect). Similarly, the capabilities are related to the PV planning in order to identify the suitability of a region to host PV parks or a building roof to produce adequate energy, taking into account the atmospheric and surrounding effects (e.g., the shadow in an urban environment).

On the other hand, the limitations are mostly related to the available spatial and temporal resolution observed by satellites and models of atmospheric parameters that affect the PV panel efficiency under clear and all sky conditions alongside with the accuracy of the simulated PV characteristics (e.g., panel materials and spectral response, the inclination and the orientation calculation, the temperature effect on PV efficiency, the dust deposition etc.). It is important to understand that the limited ability of the simulations to represent the PV production reality is directly related to the used data uncertainties as well as the model's ability to handle a portion of the solar irradiation effects by clouds and aerosol since we just incorporate the COT and AOD and not the complete optical and physical characteristics, i.e., the cloud effective radius, the cloud phase and type, the Ångström and single scattering albedo for the aerosols. As a result, the modern EO data and techniques are able to actively support the PV energy producers in any solar system scale and the produced electricity handling entities (e.g., transmission and distribution system operators) by using the provided information taking always into account that the outputs are simulations accompanied with a wide range of uncertainties.

The limitations have to do with the accuracy and resolution of the EO data which have to be even more reliable and highly resolution in the future in order to quantify even better the atmospheric parameters that affect solar energy production.

4. Conclusions

This study aimed for GHI estimation in conjunction with PV power production with modelled ones by exploiting exclusively the EO data on clouds and aerosols. To this direction, AOD products from CAMS are used for the quantification of the aerosols effect on GHI, and COT from MSG is used for the quantification of cloud effect. With the year-long analysis of AMF and CMF from Figure 6 we found that cloud is the most limiting parameter for solar energy production. The impact of aerosols and clouds on solar energy production is presented in [17,24] where Earth Observation data sources were used for continuous monitoring, modelling and forecasting of these parameters, none of these parameters were accurately measured using the real time ground-based measurements. At Thanagazi location, the monthly (January–December) average attenuation in GHI due to aerosol is observed between 4.8% to 9.4% whereas due to cloud the percentage attenuation in GHI is observed between 2% to 24%. On an annual basis, cloud reduces the GHI by 10%, whereas aerosol reduces the GHI by 6% and has a significant impact on PV power generation and profit from PV installations. Indicatively, for a 1175 kW of PV power installation, the average FL due to cloud is 1647 K INR. The FL due to aerosol for the same installation is 828 K INR. Hence, the results of this study highlight the nowadays capabilities of EO to realistically capture the PV production in conjunction with the limitations of the EO accuracy and resolution to precisely quantify the atmospheric parameter effect. In the future, it will be interesting to carry out such a study for different locations in India for accurate measurement of aerosol and cloud parameter using EO data and ground based real time measurements.

Author Contributions: P.K. designed and conceptualized the idea for this study; A.K. and P.K. analyzed the data, prepared the graphs and wrote the manuscript; Y.K. and P.K. supervised A.K.; A.K., Y.K. and R.G. collected roof-top PV data and other required data for plant location. A.K., P.K., Y.K. and R.G. reviewed the manuscript; All authors have read and agreed to the published version of the manuscript.

Funding: This research received no external funding.

Data Availability Statement: CAMS data can be obtained from the Copernicus data center (https://atmosphere.copernicus.eu/data accessed on 9 June 2023). MSG based observations can be obtained from the EUMETSAT (https://atmosphere.copernicus.eu/data accessed on 9 June 2023).

Acknowledgments: A.K., P.K., Y.K. and R.G acknowledge the Copernicus, EUMETSAT. SAFNWC and solar farm in Rajasthan for providing the data of aerosols, clouds and solar irradiance. P.K. acknowledges the Eiffel project under grant agreement 101003518.

Conflicts of Interest: The authors declare no conflict of interest.

References

1. Owusu, P.A.; Asumadu-Sarkodie, S. A review of renewable energy sources, sustainability issues and climate change mitigation. *Cogent Eng.* **2016**, *3*, 1167990. [CrossRef]
2. Gielen, D.; Boshell, F.; Saygin, D.; Bazilian, M.D.; Wagner, N.; Gorini, R. The role of renewable energy in the global energy transformation. *Energy Strateg. Rev.* **2019**, *24*, 38–50. [CrossRef]
3. Charles Rajesh Kumar, J.; Majid, M.A. Renewable energy for sustainable development in India: Current status, future prospects, challenges, employment, and investment opportunities. *Energy Sustain. Soc.* **2020**, *10*, 1–36. [CrossRef]
4. Kumar, S.; Madlener, R. CO_2 emission reduction potential assessment using renewable energy in India. *Energy* **2016**, *97*, 273–282. [CrossRef]
5. Zabeltitz, C.H.R.V.O.N. Effective Use of Renewable Energies for Greenhouse Heating. *Renew. Energy* **1994**, *5*, 479–485. [CrossRef]
6. Vourdoubas, J. Overview of Heating Greenhouses with Renewable Energy Sources a Case Study in Crete- Greece. *J. Agric. Environ. Sci.* **2015**, *4*, 70–76. [CrossRef]
7. Dumka, U.C.; Kosmopoulos, P.G.; Patel, P.N. Can Forest Fires Be an Important Factor in the Reduction in Solar Power Production in India? *Remote Sens.* **2022**, *14*, 549. [CrossRef]
8. Charles Rajesh Kumar, J.; Vinod Kumar, D.; Majid, M.A. Wind energy programme in India: Emerging energy alternatives for sustainable growth. *Energy Environ.* **2019**, *30*, 1135–1189. [CrossRef]
9. Dimock, M.E. National Electricity Planning. *Br. Public Util. Natl. Dev.* **2019**, *I*, 195–227. [CrossRef]
10. Ellabban, O.; Abu-Rub, H.; Blaabjerg, F. Renewable energy resources: Current status, future prospects and their enabling technology. *Renew. Sustain. Energy Rev.* **2014**, *39*, 748–764. [CrossRef]
11. Capellán-Pérez, I.; De Castro, C.; González, L.J.M. Dynamic Energy Return on Energy Investment (EROI) and material requirements in scenarios of global transition to renewable energies. *Energy Strategy Rev.* **2019**, *26*, 100399. [CrossRef]
12. International Renewable Energy Agency. *Renewable Energy Prospects for India*; International Renewable Energy Agency: Rome, Italy, 2015; ISBN 9789292600266.
13. Sharma, N.K.; Tiwari, P.K.; Sood, Y.R. Solar energy in India: Strategies, policies, perspectives and future potential. *Renew. Sustain. Energy Rev.* **2012**, *16*, 933–941. [CrossRef]
14. Energy Statistics of India 2023. Available online: https://www.mospi.gov.in/sites/default/files/publication_reports/Energy_Statistics_2023/Chapter%206-Consumption%20of%20Energy%20Resources.pdf (accessed on 28 May 2023).
15. Masoom, A.; Kosmopoulos, P.; Bansal, A.; Kazadzis, S. Solar energy estimations in india using remote sensing technologies and validation with sun photometers in urban areas. *Remote Sens.* **2020**, *12*, 254. [CrossRef]
16. Masoom, A.; Kosmopoulos, P.; Bansal, A.; Gkikas, A. Forecasting dust impact on solar energy using remote sensing and modeling techniques. *Sol. Energy* **2021**, *228*, 317–332. [CrossRef]
17. Dumka, U.C.; Kosmopoulos, P.G.; Ningombam, S.S.; Masoom, A. Impact of aerosol and cloud on the solar energy potential over the central gangetic himalayan region. *Remote Sens.* **2021**, *13*, 3248. [CrossRef]
18. Solar/Green Cities | Ministry of New and Renewable Energy | Government of India. Available online: https://mnre.gov.in/solar-cities (accessed on 26 May 2023).
19. Rahiman, R.; Yenneti, K.; Panda, A. *Making Indian Cities Energy Smart*; The Energy and Resources Institute: New Delhi, India, 2019. Available online: http://teriin.org/sites/default/files/2019-04/Making-Indian-Cities-Energy-Smart_UNSW-TERI.pdf (accessed on 26 May 2023).
20. Ramanathan, V.; Chung, C.; Kim, D.; Bettge, T.; Buja, L.; Kiehl, J.T.; Washington, W.M.; Fu, Q.; Sikka, D.R.; Wild, M. Atmospheric brown clouds: Impacts on South Asian climate and hydrological cycle. *Proc. Natl. Acad. Sci. USA* **2005**, *102*, 5326–5333. [CrossRef]
21. Dirnberger, D.; Blackburn, G.; Müller, B.; Reise, C. On the impact of solar spectral irradiance on the yield of different PV technologies. *Sol. Energy Mater. Sol. Cells* **2015**, *132*, 431–442. [CrossRef]
22. Deng, J.; Zhang, Y.; Qin, B.; Shi, K. Long-term changes in surface solar radiation and their effects on air temperature in the Shanghai region. *Int. J. Climatol.* **2015**, *35*, 3385–3396. [CrossRef]
23. Kosmopoulos, P.G.; Kazadzis, S.; Taylor, M.; Athanasopoulou, E.; Speyer, O.; Raptis, P.I.; Marinou, E.; Proestakis, E.; Solomos, S.; Gerasopoulos, E.; et al. Dust impact on surface solar irradiance assessed with model simulations, satellite observations and ground-based measurements. *Atmos. Meas. Tech.* **2017**, *10*, 2435–2453. [CrossRef]
24. Yang, J.; Yi, B.; Wang, S.; Liu, Y.; Li, Y. Diverse cloud and aerosol impacts on solar photovoltaic potential in southern China and northern India. *Sci. Rep.* **2022**, *12*, 19671. [CrossRef]
25. Roebeling, R.A.; Feijt, A.J.; Stammes, P. Cloud property retrievals for climate monitoring: Implications of differences between Spinning Enhanced Visible and Infrared Imager (SEVIRI) on METEOSAT-8 and Advanced Very High Resolution Radiometer (AVHRR) on NOAA-17. *J. Geophys. Res. Atmos.* **2006**, *111*, D20. [CrossRef]
26. Derrien, M.; Gléau, H.; Fernandez, P. *Algorithm Theoretical Basis Document for "Cloud Products" (CMa-PGE01 v3.2, CT-PGE02 v2.2 & CTTH-PGE03 v2.2)*; NWC SAF: Madrid, Spain, 2013.
27. Data | Copernicus. Available online: https://atmosphere.copernicus.eu/data (accessed on 4 April 2023).
28. Mayer, B.; Kylling, A. Technical note: The libRadtran software package for radiative transfer calculations—Description and examples of use. *Atmos. Chem. Phys.* **2005**, *5*, 1855–1877. [CrossRef]

29. Emde, C.; Buras-Schnell, R.; Kylling, A.; Mayer, B.; Gasteiger, J.; Hamann, U.; Kylling, J.; Richter, B.; Pause, C.; Dowling, T.; et al. The libRadtran software package for radiative transfer calculations (version 2.0.1). *Geosci. Model Dev.* **2016**, *9*, 1647–1672. [CrossRef]
30. Mayer, B.; Kylling, A.; Emde, C.; Buras, R.; Hamann, U.; Gasteiger, J.; Richter, B. *libRadtran User's Guide*; Meteorological Institute Munich: Munich, Germany, 2017.
31. Ménard, L.; Nüst, D.; Ngo, K.M.; Blanc, P.; Jirka, S.; Masó, J.; Ranchin, T.; Wald, L. Interoperable Exchange of Surface Solar Irradiance Observations: A Challenge. In *Energy Procedia*; Elsevier Ltd.: Amsterdam, The Netherlands, 2015; Volume 76, pp. 113–120.
32. Lefèvre, M.; Blanc, P.; Espinar, B.; Gschwind, B.; Ménard, L.; Ranchin, T.; Wald, L.; Saboret, L.; Thomas, C.; Wey, E. The HelioClim-1 database of daily solar radiation at Earth surface: An example of the benefits of GEOSS Data-CORE. *IEEE J. Sel. Top. Appl. Earth Obs. Remote Sens.* **2013**, *7*, 1745–1753. [CrossRef]
33. Taylor, M.; Kosmopoulos, P.G.; Kazadzis, S.; Keramitsoglou, I.; Kiranoudis, C.T. Neural network radiative transfer solvers for the generation of high resolution solar irradiance spectra parameterized by cloud and aerosol parameters. *J. Quant. Spectrosc. Radiat. Transf.* **2016**, *168*, 176–192. [CrossRef]
34. Kosmopoulos, P.G.; Kazadzis, S.; Taylor, M.; Raptis, P.I.; Keramitsoglou, I.; Kiranoudis, C.; Bais, A.F. Assessment of surface solar irradiance derived from real-time modelling techniques and verification with ground-based measurements. *Atmos. Meas. Tech.* **2018**, *11*, 907–924. [CrossRef]
35. Stamnes, K.; Tsay, S.-C.; Wiscombe, W.; Jayaweera, K. Numerically stable algorithm for discrete ordinate-method radiative transfer in multiple scattering and emitting layered media. *Appl. Opt.* **1988**, *27*, 2502–2509. [CrossRef]
36. Fu, Q.; Liou, K.N. On the correlated k-distribution method for radiative transfer in nonhomogeneous atmospheres. *J. Atmos. Sci.* **1992**, *49*, 2139–2156. [CrossRef]
37. Zhong, W.; Li, F.; Zhang, Z.; Song, L.; Li, Z. Short fiber reinforced composites for fused deposition modeling. *Mater. Sci. Eng. A* **2001**, *301*, 125–130. [CrossRef]
38. Shettle, E.P. Models of Aerosols, Clouds and Precipitation for Atmospheric Propagation Studies. In Proceedings of the Conference on Atmospheric Propagation in the UV, Visible, IR and MM-Region and Related System Aspects, NATO Adv, Copenhagen, Denmark, 9–13 October 1989; Group for Aerosp; Res. and Dev.: Copenhagen, Denmark, 1989.
39. Kinne, S. The MACv2 aerosol climatology. *Tellus B Chem. Phys. Meteorol.* **2019**, *71*, 1–21. [CrossRef]
40. Eskes, H.J.; Velthoven, P.V.; Valks, P.J.M.; Kelder, H.M. Assimilation of GOME total-ozone satellite observations in a three-dimensional tracer-transport model. *Q. J. R. Meteorol. Soc. A J. Atmos. Sci. Appl. Meteorol. Phys. Oceanogr.* **2003**, *129*, 1663–1681. [CrossRef]
41. McClatchey, R.A.; Air Force Cambridge Research Laboratories; Office of Aerospace Research; United States Air Force. *Optical Properties of the Atmosphere*; Air Force Cambridge Research Laboratories: Cambridge, MA, USA, 1971.
42. Kneizys, F.X.; Shettle, E.P.; Gallery, W.O.; Chetwynd, J.H., Jr.; Abreu, L.W. Air Force Geophysics Lab Hanscom AFB Ma. In *Atmospheric Transmittance/Radiance: Computer Code LOWTRAN 6. Supplement: Program Listings*; Air Force Geophysics Lab Hanscom: Tampa, FL, USA, 1983.
43. Fountoulakis, I.; Papachristopoulou, K.; Proestakis, E.; Amiridis, V.; Kontoes, C.; Kazadzis, S. Effect of Aerosol Vertical Distribution on the Modeling of Solar Radiation. *Remote Sens.* **2022**, *14*, 1143. [CrossRef]
44. Photovoltaic Geographical Information System. Available online: https://re.jrc.ec.europa.eu/pvg_tools/en/ (accessed on 26 May 2023).
45. Global Solar Atlas. Available online: https://globalsolaratlas.info/map (accessed on 25 October 2022).
46. Global Monitoring Laboratory—Earth System Laboratory. Available online: https://gml.noaa.gov/ (accessed on 12 October 2022).
47. Mercom India. Available online: https://mercomindia.com/rajasthan-levelized-tariff-solar-kusum-program/ (accessed on 29 December 2022).
48. Dumka, U.C.; Kaskaoutis, D.G.; Francis, D.; Chaboureau, J.P.; Rashki, A.; Tiwari, S.; Singh, S.; Liakakou, E.; Mihalopoulos, N. The Role of the Intertropical Discontinuity Region and the Heat Low in Dust Emission and Transport over the Thar Desert, India: A Premonsoon Case Study. *J. Geophys. Res. Atmos.* **2019**, *124*, 13197–13219. [CrossRef]
49. Ben-tayeb, A.; Diouri, M.; Meziane, R.; Steli, H. Solar radiation attenuation by aerosol: Application to solar farms. *Air Qual. Atmos. Health* **2020**, *13*, 259–269. [CrossRef]
50. Iqbal, M. *An Introduction to Solar Radiation*; Elsevier: Amsterdam, The Netherlands, 2012.
51. Djafer, D.; Irbah, A.; Zaiani, M. Identification of clear days from solar irradiance observations using a new method based on the wavelet transform. *Renew. Energy* **2017**, *101*, 347–355. [CrossRef]
52. Lefevre, M.; Oumbe, A.; Blanc, P.; Espinar, B.; Gschwind, B.; Qu, Z.; Wald, L.; Schroedter-Homscheidt, M.; Hoyer-Klick, C.; Arola, A.; et al. McClear: A new model estimating downwelling solar radiation at ground level in clear-sky conditions. *Atmos. Meas. Tech.* **2013**, *6*, 2403–2418. [CrossRef]
53. Kosmopoulos, P.G.; Kazadzis, S.; El-Askary, H.; Taylor, M.; Gkikas, A.; Proestakis, E.; Kontoes, C.; El-Khayat, M.M. Earth-observation-based estimation and forecasting of particulate matter impact on solar energy in Egypt. *Remote Sens.* **2018**, *10*, 1870. [CrossRef]
54. Haney, J.; Burstein, A. *PV System Operations and Maintenance Fundamentals Solar*; SolarABCs: Belleair Bluffs, FL, USA, 2013.

55. Ramachandran, S.; Kedia, S. Aerosol-precipitation interactions over India: Review and future perspectives. *Adv. Meteorol.* **2013**, *2013*, 649156. [CrossRef]
56. Polo, J.; Zarzalejo, L.F.; Cony, M.; Navarro, A.A.; Marchante, R.; Martín, L.; Romero, M. Solar radiation estimations over India using Meteosat satellite images. *Sol. Energy* **2011**, *85*, 2395–2406. [CrossRef]